AIAA-92-0230

Dispersed-Phase Structure of Pressure-Atomized Sprays at Various Gas Densities

L.-K. Tseng, P.-K. Wu and G.M. Faeth
University of Michigan
Ann Arbor, MI

30th Aerospace Sciences Meeting & Exhibit
January 6-9, 1992 / Reno, NV

AIAA-92-0230

Dispersed-Phase Structure of Pressure-Atomized Sprays at Various Gas Densities

L.-K. Tseng,* P.-K. Wu* and G.M. Faeth+
Department of Aerospace Engineering
The University of Michigan, Ann Arbor, Michigan 48109-2140

ABSTRACT

The dispersed-phase structure of the dense-spray region of pressure-atomized sprays was studied for atomization breakup conditions, considering large-scale (9.5 mm initial diameter) water jets in still air at ambient pressures of 1, 2 and 4 atm., with both fully-developed turbulent pipe flow and nonturbulent slug flow at the jet exit. Drop sizes and velocities, and liquid volume fractions and fluxes, were measured using holography. Measurements were compared with predictions based on the locally-homogeneous flow (LHF) approximation as well as recent correlations of drop sizes after primary breakup of turbulent and nonturbulent liquids. The dispersed-flow region beyond the liquid surface was relatively dilute (liquid volume fractions less than 0.1%), with significant separated-flow effects throughout, and evidence of near-limit secondary breakup and drop deformation near the liquid surface. Turbulent primary breakup predictions were satisfactory at atmospheric pressure, where the correlation was developed, but failed to predict observed trends of decreasing drop sizes with increasing gas density due to aerodynamic effects; in contrast, the laminar primary breakup predictions successfully treated the relatively small effects of gas density for this breakup mechanism. Effects of liquid turbulence at the jet exit were qualitatively similar to single-phase flows, yielding faster mixing rates with increased turbulence levels even though drop sizes tended to increase as well. LHF predictions within the dispersed-flow region were only qualitatively correct due to significant separated-flow effects, but tended to improve as the ambient pressure and the distance from the jet exit increased.

Nomenclature

C_a	=	aerodynamic breakup constant, Eq.(8)
C_τ	=	ligament residence-time constant, Eq. (7)
d	=	injector diameter
d_p	=	drop diameter
e_p	=	volume-averaged ellipticity
f	=	mixture fraction
FDF	=	fully-developed flow
g	=	liquid flux
L	=	injector passage length
MMD	=	mass median diameter
N	=	number of drops in sample
Oh_i	=	Ohnesorge number based on length scale i, $\mu_f/(\rho_f i\sigma)^{1/2}$
r	=	radial distance
Re_d	=	jet Reynolds number, $U_o d/\nu_f$
SF^d	=	slug flow
SMD	=	Sauter mean diameter
u	=	streamwise velocity
u_p	=	streamwise drop velocity
v	=	radial velocity
V	=	sample volume
$We_{f\Lambda}$	=	integral-scale Weber number, $\rho_f u_o^2 \Lambda/\sigma$
We_g	=	spray Weber number, Eq. (2)
We_{id}	=	jet Weber number based on phase i, $\rho_i u_o^2 d/\sigma$
We_{gp}	=	drop Weber number, Eq. (3)
We^*_{gp}	=	critical drop Weber number for secondary breakup
We_{gSMD}	=	primary breakup Weber number, $\rho_g u_o^2 SMD/\sigma$
x	=	streamwise distance
α	=	liquid volume fraction
Λ	=	radial integral scale
μ	=	molecular viscosity
ν	=	kinematic viscosity
ρ	=	density
σ	=	surface tension
τ_b	=	ligament aerodynamic breakup time, Eq. (8)
τ_r	=	ligament residence time, Eq. (7)

Subscripts

f	=	liquid-phase property
fc	=	liquid core property
g	=	gas-phase property
o	=	injector exit condition

Superscripts

$\bar{(\,)}$, $\tilde{(\,)}$	=	time- and Favre-averaged mean quantities
$(\,)'$	=	time-averaged rms property

INTRODUCTION

The present study extends past work in this laboratory concerning the properties of the near-injector dense-spray region of pressure-atomized sprays.[1-6] The first phase of the investigation involved measurements of liquid volume fractions,[1] and dispersed-phase structure,[2,3] of large water jets (9.5 mm and 19.1 mm initial diameter) in still air at atmospheric pressure. Tseng et al.[4] extended the liquid volume fraction measurements to treat effects of ambient gas density by studying sprays in still air at ambient pressures of 1 - 8 atm. Additionally, mechanisms of primary breakup of both nonturbulent and turbulent liquids have been studied in air at normal temperature and pressure considering various liquids and jet exit diameters and velocities.[5,6] The objective of the present investigation was to examine the effect of varying gas densities on the dispersed phase properties of dense sprays, emphasizing conditions within the multiphase mixing layer that begins right at the jet exit for atomization breakup conditions, for test conditions similar to Tseng et al.[4]

Past work on pressure-atomized dense sprays has been discussed in several recent reviews.[7-12] Early studies emphasized breakup regimes, identifying conditions for Rayleigh, wind-induced and atomization breakup—the latter having greatest practical importance because of its wide range of operating conditions and production of small drops needed for rapid mixing.[11-15] Subsequent work concentrated on visualization of the near-injector region of the flow and definition of the properties of the liquid core, which is much like the potential core of a single-phase jet.[15-20] More recently the properties of the multiphase mixing layer surrounding the liquid core have been studied, beginning with measurements within the dilute spray region near the outer edge of this flow.[21,22]

Past work in this laboratory has largely concentrated on the properties of the near-injector region during atomization

* Graduate Assistant, Department of Aerospace Engineering, The University of Michigan, Ann Arbor, Michigan 48109-2140.

+ Professor, Department of Aerospace Engineering, The University of Michigan, Ann Arbor, Michigan 48109-2140, Fellow AIAA.

breakup, using relatively large diameter liquid jets (3.5 - 19.1 mm) to provide reasonable spatial resolution.[1-6] This has included measurements of liquid volume fraction distributions using gamma-ray absorption for water jets in air at various ambient pressures.[1,4] These results showed that mixing rates were influenced by the breakup regime, turbulence properties at the jet exit and the ambient gas density; not surprisingly, atomization breakup of initially turbulent liquid jets at large ambient gas densities yielded the fastest mixing rates. Predictions based on the locally-homogeneous flow (LHF) approximation, where relative velocities between the phases are neglected, were in good agreement with measurements for Favre-averaged mixture fractions greater than 0.85, but overestimated mixing rates at lower mixture fractions. The reasons for this behavior were explored by measuring the structure of the multiphase mixing layer at atmospheric pressure—drop sizes, phase velocities, entrainment rates, and liquid volume fractions and fluxes—using holography and phase-discriminating laser velocimetry.[2,3] The results showed significant effects of separated flow so that good performance of the LHF approximation only occurred at relatively large mixture fractions where the small velocities of the gas and small drops were not very important. The results also showed that the multiphase mixing layer was surprisingly dilute, with maximum liquid volume fractions less than 0.1%, while the change from large irregular drops near the liquid surface to small round drops near the edge of the flow implied significant effects of secondary breakup.

The most recent work in this laboratory has considered the properties of primary breakup, using holography to find drop sizes and velocities at atmospheric pressure.[5,1] Two modes of primary breakup were considered: turbulent breakup, due to distortion of the liquid surface by turbulence; and nonturbulent breakup, due to stripping of liquid from boundary layers formed on the windward side of waves along the liquid surface. Correlations of SMD after primary breakup were achieved for both modes of breakup for a variety of liquids and jet exit diameters and velocities. However, these results have not been evaluated outside the relatively narrow range of liquid/gas density ratios accessible for liquid jets in air at atmospheric pressure.

The present investigation extends the earlier work in the laboratory,[1-6] addressing effects of ambient gas density on the properties of the dispersed phase during atomization breakup. The test apparatus was the same as Ref. 4, involving observations of water jets in still air at pressures of 1, 2 and 4 atm. with both turbulent and nonturbulent jet exit conditions. Holography was used to find drop sizes and velocities, and liquid volume fractions and fluxes, within the dispersed-flow region beyond the liquid surface. Following earlier work,[1-4] predictions of flow properties using the LHF approximation were used to help assess separated-flow effects on the structure of the flow. The correlations for primary breakup properties also were evaluated for effects of varying ambient gas density.

The paper begins with descriptions of experimental methods and the main features of the LHF predictions. Then theoretical and experimental findings are discussed, treating drop properties, phase velocities secondary breakup, primary breakup, and liquid volume fractions and fluxes, in turn. The present discussion is brief; additional details and a complete tabulation of data can be found in Tseng.[23]

Experimental Methods

Apparatus. The test apparatus was identical to Tseng et al.[4] This involved a steady water jet injected vertically downward within a large windowed pressure vessel (1.5 m diameter × 4.5 m long). City water was fed to the injector using a centrifugal pump with a steady outflow of water from the bottom of the tank. The rate of water flow was adjusted using a bypass system and measured using a paddle-wheel flow meter.

The injectors were identical to past work.[1-4] Two injectors having exit diameters of 9.5 mm were used: one yielding slug flow with low turbulence intensities, the other yielding fully developed turbulent pipe flow. The slug flow injector consisted of a honeycomb flow straightener, two screens to calm the flow and a 13.6:1 area contraction designed following Smith and Wang[24] to yield uniform velocities at the exit. The fully-developed flow injector had a similar configuration with the contraction followed by a constant area passage 41 jet exit diameters long to yield nearly fully-developed turbulent pipe flow at the exit. The injectors could be traversed (with positioning accuracies of 5 μm and 0.5 mm in the horizontal and vertical directions) to accommodate the rigidly mounted holocamera.

Holocamera

The holocamera and reconstruction systems were the same as Ruff et al.,[2] except for changes needed to accommodate the relatively long object beam path (1800 mm) through the test chamber, see Tseng[23] for specific details. Measurements were obtained over $6 \times 6 \times 4$ mm^3 volumes, using at least three holograms per position. The data was spatially averaged over the width of the measuring volumes, or ± 1/2 the distance between adjacent radial positions, whichever was smaller.

Drops and other nearly spherical objects were sized by finding the maximum and minimum diameters through the centroid of the image. Assuming that the object was ellipsoidal, its diameter was taken to be the diameter of a sphere having the same volume as the ellipsoid. This procedure was not appropriate for elongated liquid elements where the centroid was outside the boundaries of the image. Then, the projected area and perimeter of the image were measured and the maximum and minimum diameters of the ellipsoid having the same crossectional area and perimeter were computed to find the effective sphere diameter as before. The ellipticity, defined as the ratio of the maximum and minimum ellipsoid diameters, was also computed for each object.

Drop velocity measurements were based on the motion of the centroid of the image and were correlated as a function of diameter using a least-squares fit. This allowed plots of drop velocities for fixed drop diameters across the width of the mixing layer while making maximum use of the data on the holograms at each position . Knowing the volume and velocities of liquid elements in the flow, liquid volume fractions and fluxes could be computed in a straightforward manner.

Measurements typically involved analysis of 150 objects at each position and pressure. Experimental uncertainties were generally dominated by sampling limitations rather than resolution of the reconstructed holograms. Experimental uncertainties (25 percent confidence) were as follows:[23] Sauter mean diameter (SMD) < 10%, volume-averaged ellipticity < 15%, liquid object velocities < 20%, liquid volume fractions < 15%, and liquid fluxes < 25%. All measurements were repeatable well within these limits.

Test Conditions

Mean flow conditions were the same for the slug and fully-developed flows, and were identical to Tseng et al.[4] This involved a water flow rate of 3.47 kg/s, an average jet exit velocity of 49.1 m/s, Re_d = 462,000, Oh_d = 0.00121, We_{fd} = 312,000, and We_{gd} = 380,760 and 1520 at pressures of 1, 2 and 4 atm. Due to limitations of the pump, this water flow rate was roughly 13% lower than the atomization breakup condition considered by Ruff et al.[1-3] for the same injectors. However, present flows were well within the atomization

breakup regime defined in Refs. 13 and 14.

Ruff et al.[1] completed laser velocimeter measurements at the jet exit for the present injectors, spanning the present operating condition. For slug flow, mean streamwise velocities were uniform over the central region and declined near the wall (within 3-5% of the injector radius), due to boundary layer growth in the nozzle passage, while rms velocity fluctuations were roughly 1% of the mean streamwise velocity over the central portion of the flow. For fully-developed flow, mean velocity distributions were in good agreement with literature values for the same Reynolds number range, while rms velocity fluctuations near the axis were somewhat larger than literature values.[25,26]

Theoretical Methods

Predictions of flow properties were limited to use of the LHF approximation similar to past work.[1-4] A detailed description of the approach is provided elsewhere.[7,23] In addition to the LHF approximation, the major assumptions of the model are as follows: steady (in the mean) axisymmetric flow with no swirl, boundary layer approximations apply, negligible kinetic energy and viscous dissipation of the mean flow, buoyancy only affects the mean flow, equal exchange coefficients of all species and phases, and negligible mass transport between the phases (no evaporation). Except for the LHF approximation, which was being evaluated, these assumptions are either conditions of the experiments or are justified by successful past use, see Refs. 4, 7 and 23. The formulation followed the conserved-scalar formalism of Lockwood and Naguib[27] but used Favre averages following Bilger.[28] Governing equations were solved for conservation of mass, streamwise momentum, mean mixture fraction, turbulence kinetic energy and the rate of dissipation of turbulence kinetic energy. The specific formulation, all empirical constants, calibration of the approach for variable density single-phase flows, the numerical computations and specification of initial conditions are described in Refs. 1, 4 and 7.

Results and Discussion

Drop Properties

Similar to earlier findings,[3,5,6] present measurements of drop size distributions correlated quite well with Simmons' universal root normal distribution function.[29] The root normal distribution is defined by two moments: the SMD and the ratio of the mass median diameter (MMD) to the SMD. Typical of past observations,[3,5,6,29] MMD/SMD = 1.2 for present turbulent and nonturbulent flows, within experimental uncertainties. Thus, the entire drop size distribution will be represented by the SMD in the following. For this distribution function, 99.7% of the spray mass is contained within the range $0.1 \leq d_p/SMD \leq 3.5$

Drop properties were measured at x/d = 6 and 25 at ambient pressures of 1, 2 and 4 atm. for both fully developed and slug flows at the jet exit. These conditions provided measurements yielding the experimental uncertainties discussed earlier. Locations farther from the jet exit, at the higher ambient pressures, had larger concentrations of drops that were difficult to analyze accurately by present methods due to excessive optical noise.

Typical distributions of drop properties across the mixing layer for fully-developed flow, illustrating flow properties for turbulent primary breakup, appear in Figs. 1-4. See Tseng[23] for similar plots at all test conditions. Figures 1-3 illustrate flow properties at pressures of 1, 2 and 4 atm. at the fixed streamwise position of x/d = 6. Figures 3 and 4 illustrate effects of increasing x/d from 6 to 25 at a fixed pressure of 4 atm. Trends of flow properties as streamwise distance and pressure change, however, were similar at other conditions, see Ruff et al.[2] for extensive results showing effects of x/d for fully-developed and slug flows at atmospheric pressure. The plots include volume-averaged ellipticity, e_p, SMD and drop velocities for d_p = 10, 50, 100 and 200 μm. The measurements are plotted as a function of r/x, which is the radial similarity variable for axisymmetric turbulent single-phase jets and plumes, however, the region considered is analogous to the mixing layer around the potential core of a single-phase jet and flow properties do not exhibit similarity in this coordinate system. The range of positions where the surface of the liquid core was observed is marked on the plots. The measurements extend from the liquid core to the outer edge of the multiphase mixing layer. LHF predictions of flow velocities are also shown on the plots.

Many of the features of volume-averaged ellipticity and SMD seen in Figs. 1-4 are similar to earlier observations of Ruff et al.[2] at atmospheric pressure, however, significant effects of increasing ambient pressure are observed as well. Thus, the largest values of e_p and SMD, caused by the presence of large and irregular liquid elements, generally are in the region of the liquid surface. With increased radial distance, however, e_p approaches unity, and the SMD decreases, representing smaller round drops near the edge of the flow. This behavior is particularly evident for results at atmospheric pressure, Fig. 1, and supports the presence of primary breakup yielding large drops which subsequently undergo secondary breakup. With increasing pressure at x/d = 6, however, e_p remains near unity, and the SMD is relatively uniform across the flow. This reflects the increased propensity for secondary breakup, and shorter secondary breakup times, for particular drop sizes and relative velocities, as the gas density increases.[3] This altered behavior at increased gas densities also is evident from the substantial reduction of SMD near the surface as the ambient pressure increases. Superficially, this suggests merging of primary and secondary breakup processes as the ambient pressure increases. However, observation of hologram reconstructions indicated that the mechanism was mainly a modification of the primary breakup mechanism itself, with increasing pressures yielding shorter ligaments protruding from the surface. This behavior implies either enhanced Rayleigh breakup, from increased strain on the ligaments, or drop stripping from the tips of ligaments, due to increased aerodynamic forces on the surface of the ligaments at higher ambient densities.

Effects of streamwise distance on e_p and SMD seen at atmospheric pressure,[2,6] still are preserved at elevated pressures for present test conditions. Thus, comparing results at x/d = 6 (Fig. 3) and 25 (Fig. 4) shows increasing e_p and SMD with increasing distance from the jet exit that is characteristic of turbulent primary breakup.[6] Smaller relative velocities, caused by faster mixing rates at elevated pressures, also are probably a factor in this behavior. These potential interactions between turbulent breakup and aerodynamic effects will be taken up later, after relative velocities and local spray Weber numbers have been quantified.

Distributions of drop velocities in Figs. 1-4 have been normalized by the mass-averaged velocity at the exit of the jet. In general, there are substantial differences between the velocities of drops of different size, with drop velocities generally overestimated near the liquid core and underestimated near the edge of the flow by the LHF predictions. This is clear evidence of significant separated flow effects, typical of past observations within dilute sprays.[2,3] Drop velocities tend to decrease with increasing radial distance (reflecting effects of longer residence times in the flow for drops farther from the surface) and reduced drop diameters (reflecting smaller velocity relaxation times of smaller drops). Increasing pressure and x/d tend to decrease velocities for particular drop sizes near the edge of the flow. This is due to reduced velocity relaxation times with increased

ambient pressures for the Reynolds numbers typical of drops in sprays. Drops near the surface are less affected by x/d increases, however, because they tend to be recently formed and have velocities representative of the liquid core which do not change significantly over the range of present observations.[4]

A surprising feature of the velocity measurements illustrated in Figs. 1-4 is that the velocities of small drops, which provide a reasonable upper bound for gas velocities, remain low and relatively uniform across the flow—particularly at atmospheric pressure and small x/d, see Fig. 1. This implies that momentum exchange between the liquid and gas is not very effective. Such behavior is caused by the relatively large velocity relaxation times of large drops which contain most of the liquid momentum. Subsequent considerations will show that liquid volume fractions are relatively low in the multiphase mixing layer, reducing available interfacial area, which also contributes to reduced momentum exchange to the gas phase. A result of this behavior is that relatively low gradients of gas velocities reduce conventional production of turbulence, while large relative phase velocities promote turbulence generation by drops, so that turbulence properties in the multiphase mixing layer near the jet exit are probably quite different from more conventional turbulent flows.[7,8]

Mean Phase Velocities

The LHF predictions yielded mass-weighted (Favre)-averaged velocities; therefore, present measurements were used to compute these velocities, similar to Ruff et al.[4] To do this, mean gas velocities were taken to be equal to the mean velocities of 5 μm diameter drops, which represents the smallest drop size that could be resolved during the holography measurements. Naturally, velocities of drops of this size only represent a potential upper bound for gas velocities because their velocity relaxation times are too large for them to be accurate seeding particles to find gas velocities. However, this effect is not very significant because the large drops contain most of the momentum of the flow. Favre-averaged velocities were found by summing over the sample volume V, containing N drops, as follows:

$$\tilde{u} = \frac{\sum_{i=1}^{N} \rho_f d_{pi}^3 u_{pi} + (6V/\pi - \sum_{i=1}^{N} d_{pi}^3)\rho_g \bar{u}_g}{\sum_{i=1}^{N} \rho_f d_{pi}^3 + (6V/\pi - \sum_{i=1}^{N} d_{pi}^3)\rho_g} \qquad (1)$$

The evaluation of Eq. (1) only involved the dispersed-flow region where drops had separated from the liquid surface. This underestimates the true Favre-averaged velocity near the liquid surface because contributions from the liquid core and attached ligaments are ignored. The correction for the volume of the drops when finding the contribution of the gas-phase to $\tilde{u}$ was not very significant for present test conditions because liquid volume fractions were relatively small, less than 0.1%, in the dispersed-flow region.

Mean phase velocities for fully-developed and slug flow jet exit conditions are illustrated in Figs. 5-8. At each streamwise station and jet exit condition, velocities are plotted as a function of r/x with ambient pressure as a parameter. Three mean velocities are shown: $\tilde{u}$, found from Eq. (1), $\bar{u}_g$ taken to be the mean time-averaged velocities of drops having a diameter of 5 μm, and the LHF predictions. Two predictions are illustrated for slug flow to indicate potential effects of the boundary layer forming along the walls of the injector passage: one for L/d = 0 where the presence of the boundary layer is ignored, and one allowing for boundary layer development for a length L/d = 5 following Schlichting,[25] see Refs. 1 and 4 for descriptions of the latter predictions. These conditions bound the range of possibilities for the present slug-flow injector.[1] Finally, the range of positions where the surface of the liquid core was observed is marked on the plots for reference purposes.

Except for two conditions which may not be representative (Fig. 6 at 4 atm. and Fig. 8 at 1 atm.) measured values of $\tilde{u}$ generally are significantly larger than $\bar{u}_g$ near the liquid surface with differences between these velocities tending to decrease with increasing radial distance, ambient pressure and x/d. Thus, the dense-spray region near the liquid surface is characterized by large relative velocities that help promote primary and secondary breakup. Mean gas velocities are relatively low, with the corresponding low mean velocity gradients and large relative velocities near the liquid surface favoring turbulence generation by drops in comparison to conventional turbulence production by mean velocity gradients, as discussed earlier.

The LHF predictions of $\tilde{u}$ are generally not very satisfactory in Figs. 5-8, because present measurements emphasize near-injector conditions where effects of separated flow remain important. Nevertheless, they tend to improve with increasing distance from the jet exit and ambient pressure. This behavior is in accord with earlier scaling arguments:[3] with improved performance with distance resulting from the increased residence times of drops in the gas phase, and with improved performance with increasing pressure resulting from generally smaller drops that have shorter velocity relaxation times. Nevertheless, the tendency toward better agreement of LHF predictions comes about because large drops generally dominate the momentum content of the flow, similar to behavior at larger liquid volume fractions where the liquid core is present.[2,4] The small drops, and probably the gas, all have velocities that are generally much smaller than $\tilde{u}$. In fact, some of the apparent improvement of LHF predictions near the edge of the flow is due to the method of plotting Figs. 5-8 because all velocities become small so that differences between them are not very apparent. Similar to the findings of Ruff et al.[3] at atmospheric pressure, Favre-averaged separated flow factors, $(\tilde{u}_f - \tilde{u}_g)/\tilde{u}_f$, generally have values greater than 0.6 for the range of present measurements.[23] Finally, there is a tendency for LHF predictions to be better for slug than fully-developed flow, aside from the two untypical conditions noted earlier. This comes about because drop sizes are generally smaller for nonturbulent than turbulent primary breakup, yielding drops having shorter velocity relaxation times.[2,5,6]

The extent of the region where the liquid core is observed is another feature of interest seen in Figs. 5-8. In general, the width of this region does not vary appreciably at a fixed x/d as the ambient pressure varies. However, the effect of liquid turbulence on the liquid core is appreciable, with turbulent jet exit conditions causing the surface of the liquid to move over a wider range of radial positions and to penetrate farther from the flow axis at a given streamwise position. This behavior is due to distortion (flapping) of the liquid core by the large scale features of the turbulence, which tends to promote mixing, just like the smaller features of the turbulence tend to promote primary breakup. That these characteristics are dominated by jet exit conditions, rather than aerodynamic effects, is supported by the relatively small effect of ambient pressure on liquid surface properties, as well as LHF predictions that indicate relatively slow changes of turbulence properties at large liquid volume fractions with increasing streamwise distance.[1,4]

Secondary Breakup

Similar to Ruff at al.,[3] the propensity for secondary breakup in the mixing layer was assessed by computing mass-averaged Weber numbers. Rather than summing over the entire drop size distribution similar to Ref. 3, however, $\tilde{We}_g$ was found from the measured values of phase velocities and SMD, as follows:

$$\tilde{We}_g = \rho_g(\tilde{u}_f - \tilde{u}_g)^2 SMD/\sigma \qquad (2)$$

This definition has the advantage that maximum values of individual drop Weber numbers

$$We_{gp} = \rho_g d_p (u_p - \bar{u}_g)^2/\sigma \qquad (3)$$

are related quite simply to $\tilde{We}_g$. In particular, $\tilde{u}_f - \tilde{u}_g$ is characteristic of the relative velocities of the largest drops, while maximum drop diameters are 3-4 times larger than the SMD for the universal root normal size distribution function. Therefore, maximum We_{gp} are roughly 3-4 times larger than $\tilde{We}_g$, while more than 50% of the mass of the spray have We_{gp} larger than $\tilde{We}_g$.

Criteria for secondary breakup largely depend on drop Weber numbers for drops having low Ohnesorge numbers and large ρ_f/ρ_g, representative of present test conditions.[3,10] One criterion for water drops accelerated by shock waves is:[10,30]

$$We_{gp} > We_{gp}^* = 6.5 - 10 \qquad (4)$$

Recent work in this laboratory for similar conditions finds $We_{gp} = 12$.[31] Slower disturbance rates for water drops falling in air also yield We_{gp}^* on the order of 10 for water drops in air.[3,32] Finally, We_{gp} on the order of unity indicates the onset of conditions where drops deform from a spherical shape after shock wave disturbances at low Ohnesorge numbers and large ρ_f/ρ_g.[31]

Distributions of $\tilde{We}_g$ are plotted as a function of r/x, with ambient pressure and jet exit conditions as parameters, in Figs. 9 and 10. As before, the range of positions of the liquid surface is shown on the plots for reference purposes.

The results in Figs. 9 and 10 show that $\tilde{We}_g$ decreases monotonically with increasing radial distance. Most of the drops at the liquid surface exceed the criterion for deformation but drops near the edge of the flow are well below this criterion. Direct observations of drop shapes from hologram reconstructions agree with behavior anticipated from the deformation criterion: deformed drops were quite prevalent near the liquid surface while drops near the edge of the flow were generally spherical. This behavior contributes to decreasing values of e_p with radial distance, approaching unity near the edge of the flow, although the presence of irregular ligament-like drops contributes to large values of e_p near the surface as well.

Results illustrated in Figs. 9 and 10 also show significant potential for near-limit secondary breakup near the liquid surface for some conditions. In particular, all conditions at atmospheric pressure, as well as all conditions at x/d = 25, involve significant fractions of drops that are unstable to secondary breakup near the liquid surface. However, drops near the edge of the flow generally have We_{gp} that are lower than the breakup criterion of Eq. (4). This supports the hypothesis that reduced SMD with increasing radial distance in Figs. 1-4 is caused by secondary breakup. Near the edge of the flow, drop stability is increased because drops in this region have had relatively long residence times in the mixing layer, which provides time needed for secondary breakup and accommodation to gas velocities.

Effects of jet exit conditions also can be seen from the results illustrated in Figs. 9 and 10. Turbulent primary breakup generally yields larger drops than nonturbulent primary breakup, while the velocities of the largest drops near the liquid surface tend to approach liquid core velocities which are essentially the same in both cases, see Figs. 5-8. Thus $\tilde{We}_g$ are largest near the liquid surface, with greatest propensity for secondary breakup for fully-developed jet exit conditions (aside from the untypical behavior at x/d = 25 and 4 atm., mentioned earlier). The tendency for processes of primary and secondary breakup to merge at elevated pressures for fully developed flow also is evident from the corresponding reduction of $\tilde{We}_g$ at the liquid surface that is particularly noticeable for fully-developed flow. This effect will be discussed in greater detail in the next section.

Primary Breakup

Turbulent Primary Breakup. Recent studies have yielded correlations of drop sizes after turbulent and nonturbulent primary breakup.[5,6] These results were developed from measurements for a variety of liquids injected into air at atmospheric pressure; therefore, it is of interest to evaluate them for potential effects of varying ambient gas density using the present measurements. This will be done in the following, beginning with turbulent breakup.

Wu et al.[6] develop an expression for the SMD after turbulent primary breakup, ignoring aerodynamic effects. The correlation is based on the projection of liquid elements from the surface by radial velocity fluctuations, relating element size and velocity to the turbulence spectrum within the inertial region. The size of elements leaving the surface is taken to be the largest turbulent scale that can complete its growth at a particular point, with the length of the element determined by Rayleigh breakup considerations. The maximum size produced by this mechanism is taken to be proportional to the integral scale. For second wind-induced and atomization breakup conditions, the resulting expression for the SMD after primary breakup is:

$$SMD/\Lambda = 0.69(x/(\Lambda\, We_{f\Lambda}^{1/2}(1 + 3\, Oh_\Lambda)))^{2/3} \qquad (5)$$

or

$$SMD = \Lambda \qquad (6)$$

whichever is smaller, where Λ is the crosstream integral scale of the flow. Notably, this expression only involves properties of the liquid phase because aerodynamic effects have been ignored.

Present measurements of SMD along the liquid surface for fully developed flow, along with the predictions of Eqs. (5) and (6), are summarized in the upper part of Table 1. The agreement between predictions and measurements at atmospheric pressure, corresponding to the range of ρ_f/ρ_g used to develop Eqs. (5) and (6), is excellent. However, the predictions do not anticipate the substantial reduction of drop sizes after primary breakup as the ambient pressure increases. The progressive reduction of SMD with increasing pressure clearly suggests the presence of aerodynamic effects that are not considered in the phenomenological theory used to develop Eqs. (5) and (6).

A curious feature of the failure of Eqs. (5) and (6) to correlate SMD after primary breakup at pressures of 2 and 4 atm. is that these expressions were developed over a wide range of We_{gd}, with resulting wide variations of aerodynamic forces; thus, the problem largely appears to be related to the variation of density ratio. Insight concerning this behavior can be obtained by considering the residence times of a typical ligament breaking away from the surface and secondary breakup times for liquid elements of comparable size, using the integral-scale limit to simplify the discussion. Taking the length of the ligament at the time it separates to be $e_p\Lambda$, and the velocity of liquid flow into the ligament to be $\bar{v}'_f$, the characteristic residence time of the ligament during its formation is

$$\tau_r = C_r e_p \Lambda/\bar{v}'_f \qquad (7)$$

where C_r is a constant on the order of unity. The mode of aerodynamic breakup of the ligaments is not known; fortunately, breakup times are relatively independent of mode.[33,34]

Adopting the correlation Ranger and Nicholls[34] for

shear breakup, and taking the characteristic ligament dimension to be Λ, yields the characteristic aerodynamic breakup time of the ligament, as follows:

$$\tau_b = 5C_a\Lambda(\rho_f/\rho_g)^{1/2}/u_o \quad (8)$$

where C_a is an empirical constant of order unity to allow for shape differences between drops and ligaments, and the relative velocity has been taken to be u_o, which is representative of velocity differences between ligaments extending from the surface and the local gas velocity. Solving for the ratio of Eqs. (8) and (7) then yields:

$$\tau_b/\tau_r = (5\ C_a/C_re_p)(\rho_f/\rho_g)^{1/2}(\overline{v'}_f/u_o) \quad (9)$$

Noting that turbulence properties within the liquid do not change appreciably with position, $\overline{v'}_f/u_o$ is simply the intensity of radial velocity fluctuations at the jet exit which is a constant for the fully-developed turbulent pipe flow. Thus, Eq. (9) indicates that the relative importance of aerodynamic breakup effects only depends on the density ratio, in agreement with the present measurements and the observations of Ref. 6.

Equation (9) also suggests that the transition from turbulent breakup due to liquid turbulence alone, to conditions where aerodynamic effects also are important, occurs at pressures on the order of atmospheric pressure. For example, e_p generally is in the range 2-4 at the liquid surface for turbulent breakup, see Ref. 2 and Figs. 1-4; therefore, it is reasonable to take the first factor on the right hand side of Eq. (9) to be of order unity. The radial turbulence intensity, $\overline{v'}_f/u_o$, for fully-developed turbulent pipe flow generally is in the range 0.03-0.05.[25,26] Then, at ambient pressures of 1, 2 and 4 atm. for water and air: ρ_f/ρ_g = 846, 423 and 212, yielding τ_b/τ_r = 1.2, 0.8 and 0.6 (taking the radial turbulence intensity to be 0.04). These results suggest that aerodynamic effects begin to become important at ambient pressures on the order of 1 atm., and that this transition is largely a function of density ratio, which agrees with the SMD data of Table 1. More study is needed to refine these order of magnitude considerations, however, present findings clearly show that use of Eqs. (5) and (6) to find SMD for ρ_f/ρ_g outside the range considered in Ref. 6 is not appropriate.

Nonturbulent Primary Breakup. Wu et al.[5] have developed an expression giving the SMD after primary breakup for slug flow at the jet exit. This expression is based on aerodynamic stripping of boundary layers formed on the windward side of waves along the liquid surface. For liquid Reynolds numbers based on distance from the jet exit greater than 2×10^6, which corresponds to present conditions, a fully-developed breakup regime is entered where the SMD after primary breakup is relatively independent of distance from the jet exit. Within this regime, the correlation for SMD along the surface is

$$We_{g_{SMD}} = 16(We_{gd}/Re_d^{1/2})^{0.82} \quad (10)$$

where the Weber and Reynolds numbers are based on mean jet exit velocity, assuming small variations of velocity within the liquid core and small gas velocities along the surface — the latter generally corresponding to present observations and those of Ref. 3.

Present measurements of SMD along the liquid surface for slug flow, along with the predictions of Eq. (10), are summarized in the lower part of Table 1. In this case, measured SMD are affected only slightly with increasing pressure and distance along the surface — trends that are consistent with the predictions of Eq. (10) as well as effects of distance within the fully-developed nonturbulent breakup regime observed in Ref. 5. However, the predictions do overestimate the measured SMD by roughly a factor of two which is larger than the scatter of the data used to develop Eq. (10).[5] Specific reasons for this deficiency are not known, however, processes of nonturbulent breakup are notoriously sensitive to small disturbances within the injector so that differences in the injector passage design may be a factor. In any event, unlike turbulent primary breakup, present observations of the trends of nonturbulent primary breakup with variations of ρ_f/ρ_g appear to be consistent with the observations of Ref. 5. It should be noted, however, that parameters controlling secondary breakup (see Eqs. (4) and (8)) respond more rapidly to increased gas densities than those controlling nonturbulent primary breakup (see Eq. (10)). Thus, higher pressures than considered here may involve merging of primary and secondary breakup, similar to present observations of turbulent primary breakup: this possibility should be explored.

Liquid Volume Fractions and Fluxes

Measured and predicted distributions of liquid volume fractions and fluxes are illustrated in Figs. 11 and 12 for both fully-developed and slug flow. Measurements of liquid volume fractions include both present findings, using holography, and those of Tseng et al.[4] using gamma-ray absorption for the same flows. LHF predictions for slug flow are shown at the limits L/d = 0 and 5 as before. The range of locations of the liquid surface also are indicated on the plots.

The measurements of liquid volume fractions by gamma-ray absorption generally yield larger values than those found by holography in the region where they overlap in Figs. 11 and 12. This region is associated with the presence of the liquid core; therefore, the main reason for the differences is that the holography measurements do not include the significant contributions of the liquid core and the attached ligaments protruding from its surface. Thus, the discrepancy largely reflects reduced liquid volume fractions anticipated when moving from a liquid region to a fully-dispersed multiphase flow region. Liquid volume fractions in the dispersed-flow region don't vary appreciably with increasing pressure and distance from the jet exit, with maximum values remaining at roughly 0.1%. For liquid volume fractions of this magnitude, effects of collisions are not very significant.[7] Distributions of liquid volume fractions are generally broader, with higher liquid volume fractions in the dispersed-flow region for fully-developed than slug flow. This reflects the faster mixing rates of the turbulent breakup process at the liquid surface. The LHF predictions of liquid volume fractions are reasonably good up to the outer edge of the region where the liquid surface is present, which involves liquid volume fractions greater than 0.1. Thereafter, the LHF predictions only bear a crude resemblance to measured properties in the dispersed flow region: in part because the measurements ignore the presence of the liquid surface and attached ligaments, as noted earlier; and in part, because of the significant effects of separated flow in the dispersed-flow region.

The liquid flux measurements and predictions illustrated in Figs. 11 and 12 are qualitatively similar to the liquid volume fractions. Fluxes for fully-developed flow generally are higher than for slug flow due to the faster rates of turbulent primary breakup (except for the untypical behavior for fully-developed flow at x/d = 25 and 4 atm., Fig. 12, noted earlier). Measurements of liquid fluxes do not account for contributions from the liquid core and its attached ligaments and underestimate fluxes in the region of the liquid surface as a result. Accounting for this, the LHF predictions are in qualitative agreement with the measurements, although consideration of separated-flow effects is needed to develop a quantitatively accurate methodology. There is little evidence of improved performance of the LHF approach with increasing pressure for liquid volume fractions and fluxes. The reason for this is that present measurements emphasize the near-injector region where separated-flow effects are still very significant.

Conclusions

The near-injector region of pressure-atomized sprays was investigated at various ambient gas densities, considering atomization breakup conditions for both fully-developed and slug flow at the jet exit. The main conclusions of the study are as follows:

1. Similar to earlier observations at atmospheric pressure,[2,3,5,6] drop sizes at each point satisfied Simmons' root-normal drop size distributions,[29] with an MMD/SMD ratio of 1.2. Thus, the entire drop size distribution can be characterized by a single moment, like the SMD.

2. Drop sizes after primary breakup generally were larger for fully-developed than for slug flow jet exit conditions, highlighting the importance of injector passage disturbances on spray properties. The correlation of Wu et al.[6] for SMD after turbulent primary breakup was in excellent agreement with present measurements at atmospheric pressure — the same ambient pressure used to develop the correlation. However, the correlation did not represent measured trends of reduced SMD after primary breakup as the ambient pressure increased. This suggests the presence of aerodynamic effects, or merging of primary and secondary breakup, that were not considered when the correlation was developed. The difficulty is largely associated with an effect of density ratio; therefore, the correlation of Ref. 6 should not be used outside the range of ρ_f/ρ_g originally used to define it.

3. Measured trends of effects of ambient pressure and distance from the injector on SMD after nonturbulent primary breakup were in good agreement with the correlation developed by Wu et al.[5] which includes consideration of aerodynamic effects. This implies relatively small effects of ambient pressure on drop sizes after nonturbulent primary breakup so that merging of primary and secondary breakup at higher pressures may still be a factor, due to the larger response of secondary breakup processes to changes in gas density: this potential limitation requires additional study before the correlation of Ref. 5 can be applied confidently to high-pressure sprays.

4. Spray Weber numbers after primary breakup imply that a significant fraction of the drops will undergo near-limit secondary breakup (particularly at low pressures and far from the injector) while most of the drops exceed conditions where they deform from a spherical shape even if they do not undergo secondary breakup. Drops near the edge of the flow, however, have Weber numbers well below values associated with secondary breakup and deformation. These trends were generally in accord with measured radial variations of drop sizes and shapes.

5. Similar to earlier observations at atmospheric pressure,[2] liquid volume fractions in the dispersed-flow region beyond the liquid surface were relatively low, less than 0.1%. Thus, the flow in this region corresponds to a dilute spray, aside from added complications of secondary breakup and irregular or deformed drops.

6. Favre-averaged separated flow factors, $(\tilde{u}_f-\tilde{u}_g)/\tilde{u}_f$, were generally greater than 0.6 throughout the dispersed flow region, implying significant effects of separated flow and surprisingly low gas velocities even near the liquid surface. These effects suggest that turbulence generation by drops,[7,8] is a major feature of the dispersed flow region.

7. Predictions based on the LHF approximation were only qualitatively useful due to significant separated-flow effects in the dispersed-flow region. Performance of the LHF approach, however, tended to improve with increasing liquid volume fractions, ambient pressure and distance from the injector. Pending resolution of existing uncertainties about the properties of primary and secondary breakup, the LHF approach offers a useful treatment of sprays in the atomization breakup regime at high ambient pressures where drop sizes are likely to be small. It should be recognized, however, that the LHF approach will overestimate the rate of development of the flow by a degree that cannot be quantified until uncertainties about breakup and other properties of the near-injector region are resolved.

Acknowledgements

This research was sponsored by the Office of Naval Research Grant No. N00014-89-J-1199 under the technical management of G. D. Roy; initial apparatus development was sponsored by the Air Force Office of Scientific Research, Grant No. 89-0516 with J. M. Tishkoff serving as technical manager. The U.S. Government is authorized to reproduce and distribute copies for governmental purposes notwithstanding any copyright notation thereon.

References

[1]Ruff, G.A., Sagar, A.D. and Faeth, G.M., "Structure of the Near-Injector Region of Pressure-Atomized Sprays," *AIAA J.*, Vol. 27, July 1989, pp. 549-559.

[2]Ruff, G.A., Bernal, L.P. and Faeth, G.M., "Structure of the Near-Injector Region of Non-Evaporating Pressure-Atomized Sprays," *J. Prop. Power*, Vol. 7, Mar.-April 1991, pp. 221-230.

[3]Ruff, G.A., Wu, P.-K., Bernal, L.P. and Faeth, G.M., "Continuous- and Dispersed-Phase Structure of Dense Nonevaporating Pressure-Atomized Sprays," *J. Prop. Power*, in press.

[4]Tseng, L.-K., Ruff, G.A. and Faeth, G.M., "Effects of Gas Density on the Structure of Liquid Jets in Still Gases," *AIAA Journal*, in press.

[5]Wu, P.-K., Ruff, G.A. and Faeth, G.M., "Primary Breakup in Liquid/Gas Mixing Layers," *Atomization and Sprays*, in press.

[6]Wu, P.-K., Tseng, L.-K., and Faeth, G.M., "Primary Breakup of Turbulent Liquids," AIAA Paper No. 92-0462, 1992.

[7]Faeth, G.M., "Mixing, Transport and Combustion in Sprays," *Prog. Energy Combust. Sci.*, Vol.13, 1987, pp. 293-345.

[8]Faeth, G.M., "Structure and Atomization Properties of Dense Turbulent Sprays," *Twenty-Third Symposium (International) on Combustion*, The Combustion Institute, 1990, Pittsburgh, pp. 1345-1352.

[9]Chigier, N.A., "The Physics at Atomization," *Proceedings of the Fifth International Conference on Liquid Atomization and Spray Systems*, NIST SP-813, National Institute of Standards and Technology, Washington, July 1991, pp. 1-15.

[10]Clift, R., Grace, J.R. and Weber, M.E., *Bubbles, Drops and Particles*, Academic Press, New York, 1978, p. 346.

[11]Reitz, R.D. and Bracco, F.V., "Mechanism of Atomization of a Liquid Jet," *Phys. Fluids*, Vol. 25, Oct. 1982, pp. 1730-1742.

[12]Reitz, R.D., "Atomization and Other Breakup Regimes of a Liquid Jet," Ph.D. Dissertation No. 1375-T, Princeton University, Princeton, New Jersey, 1978.

[13]Miesse, C.C., "Correlation of Experimental Data on the Disintegration of Liquid Jets," *Ind. Engr. Chem.*, Vol. 47, Sep. 1955, pp. 1690-1697.

[14]Ranz, W.E., "Some Experiments on Orifice Sprays," *Can. J. Chem. Engr.*, Vol. 36, Aug. 1958, pp. 175-181.

[15]Phinney, R.E., "The Breakup of a Turbulent Jet in a Gaseous Atmosphere," *J. Fluid Mech.*, Vol. 6, Oct. 1973, pp. 689-701.

[16]Hoyt, J.W. and Taylor, J.J., "Waves on Water Jets," *J. Fluid Mech.*, Vol. 88, 1977, pp. 119-127.

[17]Hoyt, J.W. and Taylor, J.J., "Turbulence Structure in a Water Jet Discharging in Air," *Phys. Fluids*, Vol. 20 (Pt. II), 1977, pp. S253-S257.

[18]Hoyt, J.W. and Taylor, J.J., "Effect of Nozzle Boundary Layer on Water Jets Discharging in Air," *Jets and Cavities* (J.H. Kim, O. Furuya and B.R. Parkin, ed.) ASME-FED, Vol. 31, ASME, New York, 1985, pp. 93-100.

[19]Hiroyasu, H., Shimizu, M., and Arai, M., "The Breakup of a High Speed Jet in a High Pressure Gaseous Environment," Univ. Of Wisconsin, Madison, ICLASS-82, 1982.

[20]Chehroudi, B., Onuma, Y., Chen, S.-H. and Bracco, F. V., "On the Intact Core of Full Cone Sprays," SAE Paper No. 850126, 1985.

[21]Wu, K.-J., Su, C.-C., Steinberger, R.L., Santavicca, D.A. and Bracco, F.V., "Measurements of the Spray Angle of Atomizing Jets," *J. Fluids Engr.*, Vol. 105, Dec. 1983, pp. 406-415.

[22]Wu, K.-J., Coghe, A., Santavicca, D.A. and Bracco, F.V., "LDV Measurements of Drop Velocity in Diesel-Type Sprays," *AIAA. J.* Vol. 22, Sept. 1984, pp. 1263-1270.

[23]Tseng, L.-K., "Near-Injector Structure of Non-Evaporating Pressure-Atomized Sprays at Various Ambient Densities," Ph.D. Thesis, The University of Michigan, Ann Arbor, Michigan, 1991.

[24]Smith, R.H. and Wang, C.-T., "Contracting Cones Giving Uniform Throat Speeds," *J. Aero. Sci.*, Vol. 11, Oct. 1944, pp. 356-360.

[25]Schlichting, H., *Boundary Layer Theory*, 7th ed., McGraw-Hill, New York, 1979, p. 599.

[26]Hinze, J.O., *Turbulence*, 2nd ed., McGraw-Hill, New York,1975, pp. 427 and 724-734.

[27]Lockwood, F.C. and Naguib, A.S., "The Prediction of Fluctuations in the Properties of Free, Round-Jet Turbulent Diffusion Flames," *Combust. Flame*, Vol. 24, Feb. 1975, pp. 109-124.

[28]Bilger, R.W., "Turbulent Jet Diffusion Flames," *Prog. Energy Combust. Sci.*, Vol. 1, 1976, pp. 87-109.

[29]Simmons, H.C., "The Correlation of Drop Size Distributions in Fuel Nozzle Sprays," *J. Engrg. for Power*, Vol. 99, July 1977, pp. 309-319.

[30]Krzeczkowski, S.A., "Measurement of Liquid Droplet Disintegration Mechanisms," *Int. J. Multiphase Flow*, Vol. 6, 1980, pp. 227-239.

[31]Hsiang, L.-P. and Faeth, G.M., "Secondary Drop Breakup in the Deformation Regime," AIAA Paper No. 92-0110, 1992.

[32]Pruppacker, H.R. and Klett, J.D., *Microphysics of Clouds and Precipitation*, D. Reidel Publishing Co., Boston, 1978, pp. 123-456.

[33]Borisov, A.A., Gel'fand, B.E., Natanzon, M.S. and Kossov, O.M., "Droplet Breakup Regimes and Criteria for Their Existence," *Inzh.-Fiz. Zh.*, Vol. 40, Jan. 1981, pp. 64-70.

[34]Ranger, A.A. and Nicholls, J.A., "Aerodynamic Shattering of Liquid Drops," *AIAA J.*, Vol. 7, Feb. 1969, pp. 285-290.

Table 1 Measured and predicted SMD (μm) along liquid surface[a]

Pressure (atm.)	1		2		4	
x/d	Meas.	Pred.	Meas.	Pred.	Meas.	Pred.
Fully-Developed Flow:[b]						
6	343	374	133	374	70	374
25	940	968	343	968	157	968
Slug Flow:[c]						
6	117	241	100	213	98	188
25	143[d]	215[d]	140	213	138	188

[a]Momentum averaged injection velocity (m/s) of 40[b], 48[c] and 56[d].

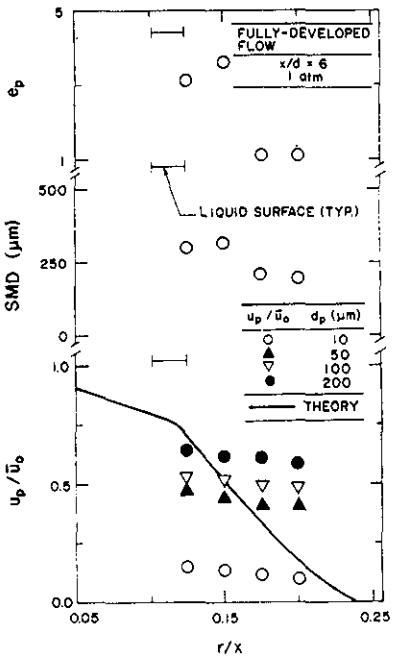

Fig. 1 Dispersed-phase properties for fully-developed flow at x/d = 6 and 1 atm.

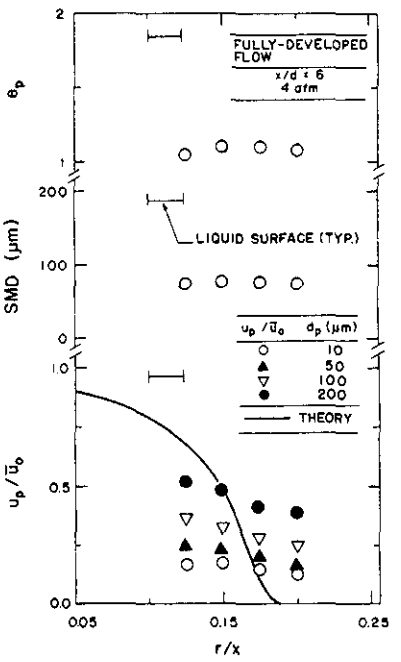

Fig. 3 Dispersed-phase properties for fully-developed flow at x/d = 6 and 4 atm.

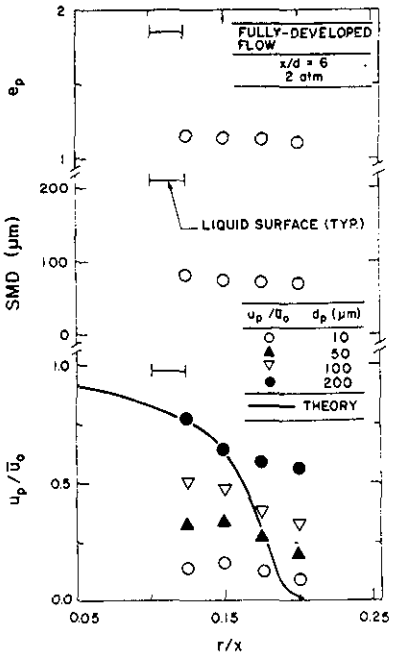

Fig. 2 Dispersed-phase properties for fully-developed flow at x/d = 6 and 2 atm.

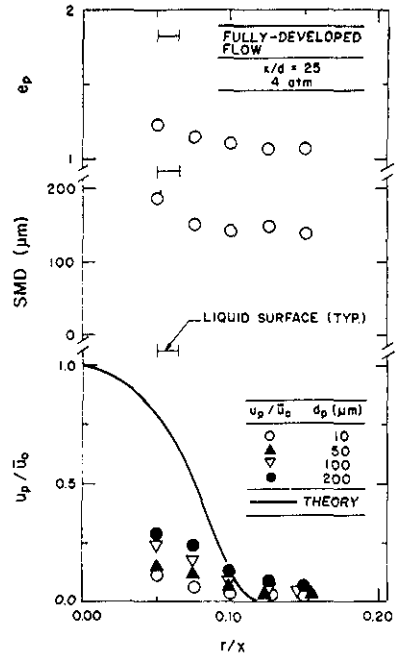

Fig. 4 Dispersed-phase properties for fully-developed flow at x/d = 25 and 4 atm.

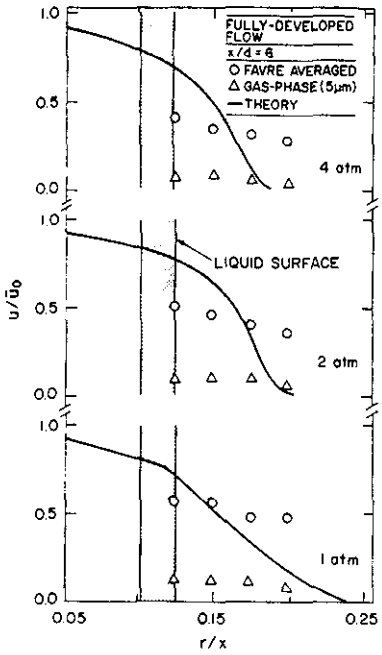

Fig. 5 Mean-phase velocities for fully-developed flow at x/d = 6.

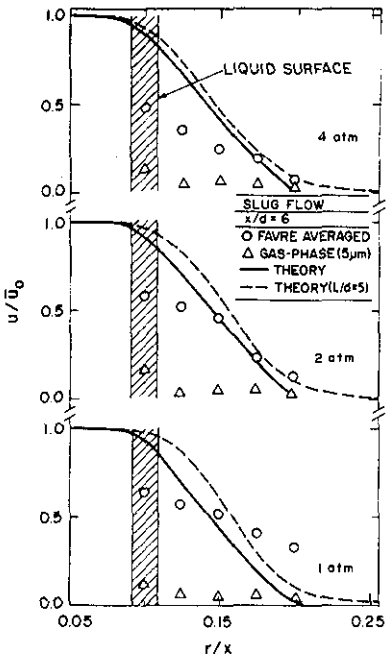

Fig. 7 Mean-phase velocities for slug flow at x/d = 6.

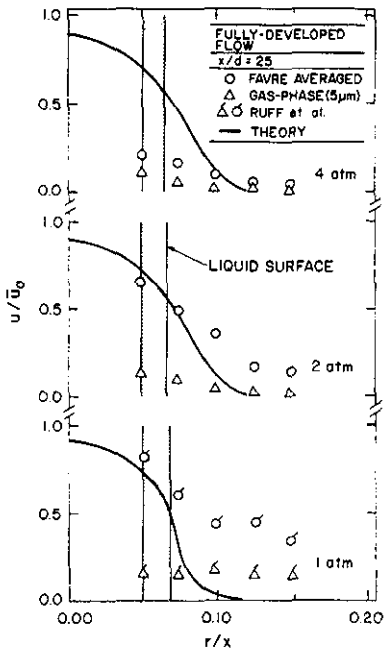

Fig. 6 Mean-phase velocities for fully-developed flow at x/d = 25.

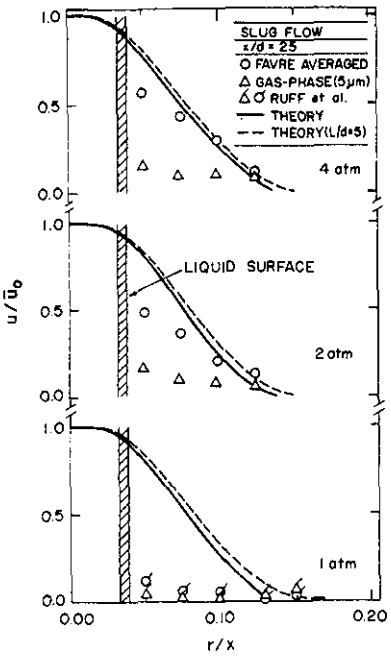

Fig. 8 Mean-phase velocities for slug flow at x/d = 25.

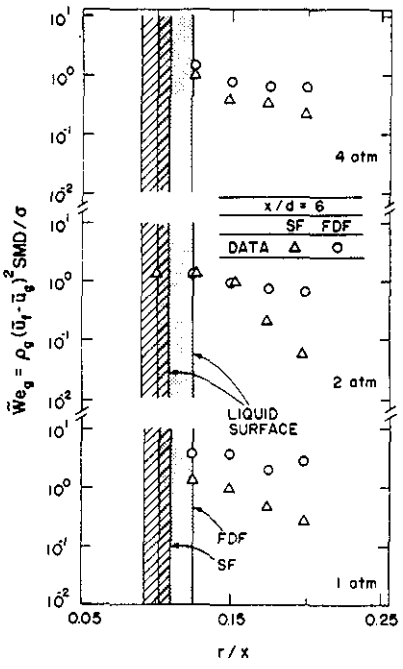

Fig. 9 Favre-averaged drop Weber numbers for fully-developed and slug flow at x/d = 6.

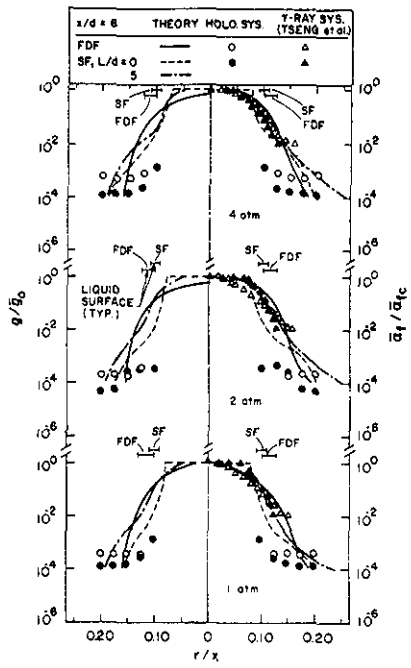

Fig. 11 Liquid volume fractions and fluxes for fully-developed and slug flow at x/d = 6.

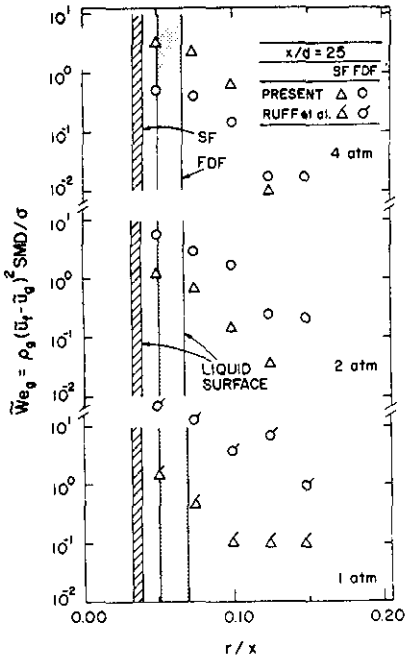

Fig. 10 Favre-averaged drop Weber numbers for fully-developed and slug flow at x/d = 25.

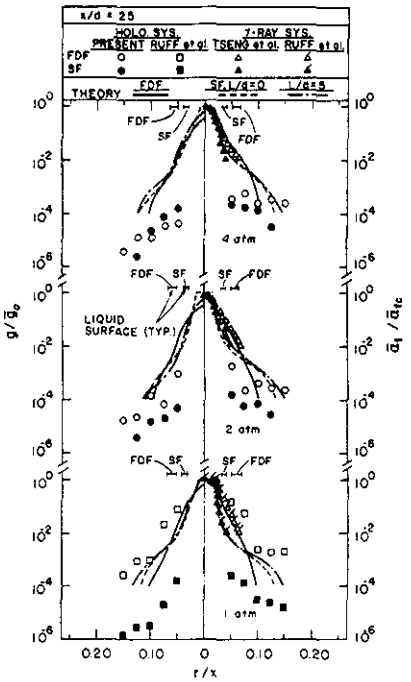

Fig. 12 Liquid volume fractions and fluxes for fully-developed and slug flow at x/d = 25.